

Delay-Doppler map (DDM) distortions induced by specular point location estimate inaccuracies

Giuseppe Grieco (1), Ad Stoffelen (1), Marcos Portabella (2)

- 1) Koninklijk Nederlands Meteorologisch Instituut, De Bilt, The Netherlands
- 2) Institut de Ciències del Mar (ICM-CSIC), Barcelona, Spain

Abstract

The impact of specular point location estimate inaccuracies on satellite delay-Doppler map (DDM) observed distortions is assessed in this paper. A set of raw reflected Global Navigation Satellite System (GNSS-R) echoes acquired by the satellite constellation Cyclone GNSS (CYGNSS) during hurricanes Irma and Harvey has been recompressed by progressively reducing the Doppler frequency inaccuracy at the specular point. The results show that recompressing raw echoes with highly accurate specular point location estimates strongly reduces the DDM distortions.

INTRODUCTION

Global Navigation Satellite System Reflectometry (GNSS-R) has proven to be an effective tool for ocean surface wind speed retrieval (Zavorotny, 2000). Satellite GNSS-R is becoming more and more appealing to the weather forecast community, especially for its low cost and for its potential to cover time lags of scatterometers (Cardinali, 2009). At the moment, two missions are being operated with the aim of demonstrating the feasibility of satellite GNSS-R wind field retrievals: the polar orbiting platform TechDemoSat-1 (TDS-1) (Foti, 2015), launched in 2014, and the Cyclone GNSS (CYGNSS) constellation (Clarizia, 2014), deployed at the end of 2016. However, to the best of our knowledge, GNSS-R wind speed retrieval accuracy is still far from a suitable performance for data assimilation into Numerical Weather Prediction (NWP) models. The GNSS-R wind speed operational retrieval algorithms exploit the delay-Doppler map (DDM) peak (for TDS-1) (Foti, 2015) or a combination of two observables: the Leading Edge Slope (LES) and the average of the delay-Doppler bins around the DDM peak (DDMA) (for CYGNSS) (Clarizia, 2014). The consequence of such choices is that most of the information contained in the DDM is discarded. Other approaches are based on the use of different observables (Rodríguez-Alvarez, 2016), on data assimilation techniques, or on the exploitation of the free ambiguity area of the DDM (Tye, 2016), the so-called “horse shoe” (HS). The latter is also known as “stare processing”. It consists of a non-coherent multi look approach aiming at properly merging the Bistatic Normalized Radar Cross Section (σ_0) relative to a given target area acquired during a series of 1 Hz DDMs. Indeed, a given target area is in the field of view (FOV) of the GNSS receiver for a time interval long enough to be sounded with different acquisition geometries. Targets lying along the nadir flight track of the receiver are mapped onto the DDM HS. Figure 1 shows and illustration of the DDM HS sampling.

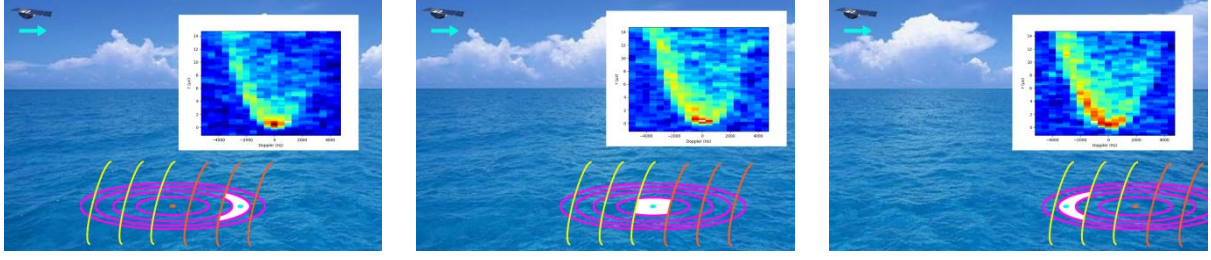


Figure 1: Illustration of the DDM horse shoe sampling. The effective sounded area (white patch) relative to a given target point (cyan point) at a given instant of time, is mapped onto the white pixel of the DDM (top right of each plot). The violet ellipses represent the iso-delay lines, while the parabolic lines represent the iso-Doppler lines, positive in orange and negative in yellow. The central plot represents the instant of time when the target point perfectly overlaps the specular point (SP, orange point), while the left (right) plot refers to a preceding (successive) instant of time.

The stare processing relies on the possibility of calibrating the σ_0 along the entire DDM HS. This can be achieved by inverting the approximated Bistatic Radar Equation (BRE), which reads as follows:

$$P_R \simeq \frac{\lambda^2 P_T D_T D_R \sigma_0 A}{(4\pi)^3 L_1 L_0 R_0^2 R_1^2} \quad 1$$

where P_R and P_T are respectively the received and the transmitted power, D_R and D_T are, respectively, the receiver and the transmitter antenna gains, R_0 and R_1 are, respectively, the receiver-target and the transmitter-target ranges, L_0 and L_1 are the atmospheric losses on the receiver-target and the transmitter-target paths, respectively, λ is the carrier frequency wavelength, and A is the effective sounded area. The accuracy of each factor involved in equation 1 affects the accuracy of the HS σ_0 calibration. All of them come from metadata (D_R , D_T , R_0 , R_1 , P_T and λ), from atmospheric composition models (L_0 and L_1) and from simulation models of the acquisition geometry (A). It has been recently found that regular TDS-1 DDMs are affected by some distortions, whose main cause is attributable to inaccuracies of the specular point (SP) location estimate (Grieco, 2018). Indeed, the SP location is a key ingredient for compressing the raw echo in the DDM. (Grieco, 2018) reveal DDM deformations after applying a quality control (QC) scheme specifically designed for such purpose. Such deformations have a high correlation ($\rho = 0.93$) with the Doppler difference between the SP location estimate used for DDM compression and the SP location estimate obtained by means of more accurate Earth surface models. The aim of this paper is to demonstrate that the inaccuracy of the SP location estimate is the main cause of the DDM distortions. The paper is organized as follows: in section DATASET AND METHODOLOGY the dataset of raw CYGNSS echoes and the methodology used are described. Finally, the experimental results together with some conclusion remarks can be found in section RESULTS AND DISCUSSION.

DATASET AND METHODOLOGY

Two 60 seconds tracks of the CYGNSS mission over hurricanes Harvey (July 25th 2018) and Irma (September 8th 2018) have been used in this analysis. The only reason for selecting extreme event cases is that CYGNSS raw data are only available under those conditions, and only for scientific purposes. For the sake of completeness, Figures 2 and 3 show a synoptic view of both hurricanes at the acquisition times of DDMs. We have selected these two cases because the Doppler frequency errors (shifts) at the SP are one order of magnitude different, being around 150 Hz for Harvey and around 10-20 Hz for Irma. This way, we can check whether the DDM distortion magnitudes are different.

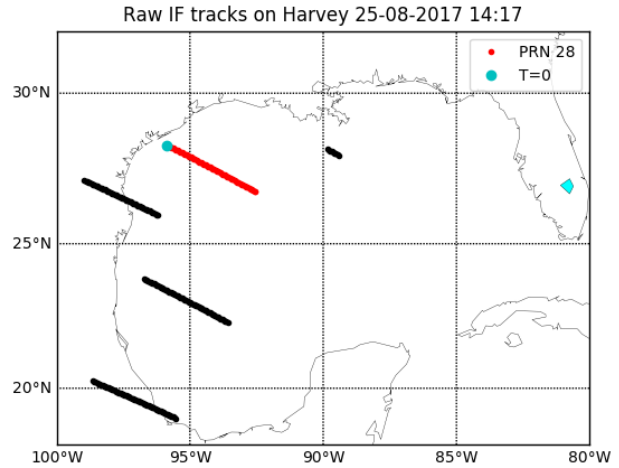
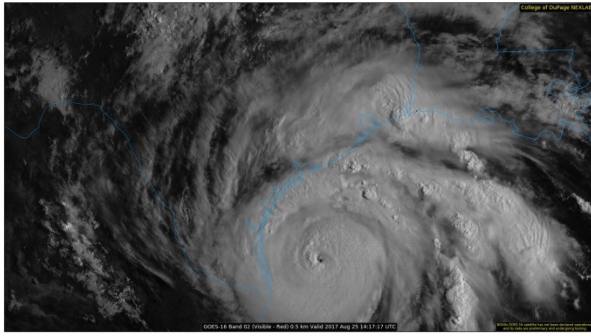


Figure 2: Left: synoptic view of the Hurricane Harvey on the 25th of August 2017 at 14:17 UTC from GOES-16, O₂ band. Right: specular point position relating to the GPS transmitters tracked by CYGNSS at the same time. The red track refers to the one that has been analysed in this paper. The black tracks represent the other GPS satellites that have been tracked by the GNSS receiver in the same time interval.

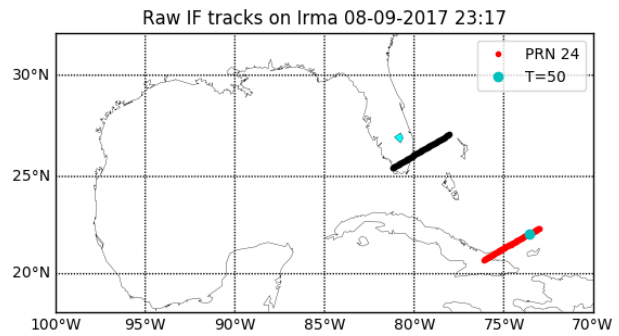
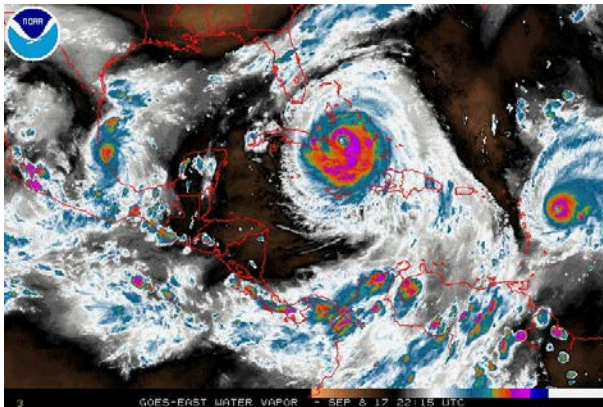


Figure 3: Left: synoptic view of the Hurricane Irma on the 8th of September 2017 at 17:22 UTC from GOES-East, water vapour band. Right: specular point position relating to the GPS transmitters tracked by CYGNSS a few hours later. The red track refers to the one that has been analysed in this paper.

Each one-second window of raw echoes is re-compressed with the same parameters used for the regular DDMs, except for the Doppler frequency at the SP. The latter is varied in a Doppler interval of $[-250,250]$ Hz centered around the most accurate estimate of the Doppler frequency at the SP, for a total of 16 values, among which there is also the on-board estimate of the Doppler frequency at the SP. We also consider the extreme values of ± 250 Hz because one of the aims of this exercise is to verify the invariance of the compressed DDMs for Doppler frequency values at the SP whose difference is an integer multiple of a regular Doppler bin size (500 Hz). In order to properly compare the re-compressed DDMs, we have computed the cross correlation coefficient (ρ) of the normalized waveforms (WFs) at ± 1 kHz, according the QC scheme presented in (Grieco, 2018). The higher the ρ , the less the distortions.

RESULTS AND DISCUSSION

It has been verified, even if only from a qualitative point of view, that the distortion magnitudes are different for the DDMs acquired during Harvey and those acquired during Irma, the former being higher (not shown). As such, it is found that CYGNSS regular DDMs are affected by the same distortions as TDS-1 DDMs (Grieco, 2018). This is an expected result since the on-board algorithm for the fast computation of the SP location is the same for both missions.

The left (right) plot of Figure 4 shows the DDM obtained with a Doppler frequency at the SP that is 250 Hz lower (higher) than its most accurate value. We verify that the difference between the two DDMs for all the overlapping Doppler channels (absolute value) is null, demonstrating that the DDM compression is invariant for Doppler frequency differences at the SP equal to integer multiples of the Doppler bin size (500 Hz). It is important to stress that the values on the x-axis of both plots are Doppler frequency values relative to the “0-Doppler” value, which is the one used for the DDM compression.

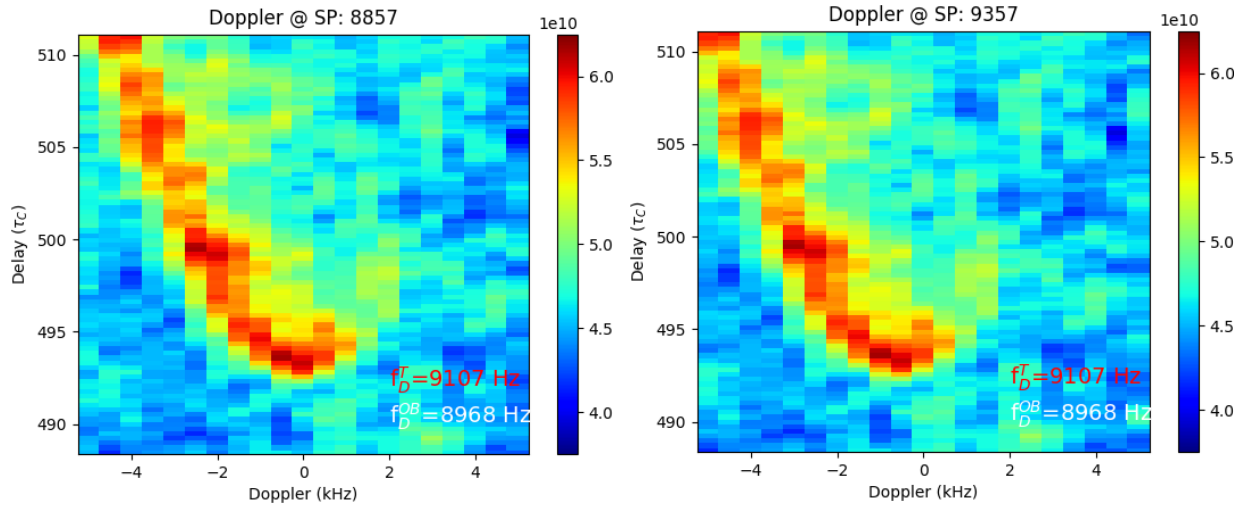


Figure 4: Left: DDM compressed with a Doppler frequency value at the specular point of 8857 Hz (250 Hz lower than the most accurate value). The most accurate value is reported in red on the plot (f_D^T), while the on-board value is stated in white (f_D^{OB}). Right: Same echo than that of the left plot but compressed with a Doppler frequency value at the specular point of 9357 Hz (500 Hz higher than on the left). It is verified that the difference between the left DDM in the Doppler interval [-5.0,4.5] Hz and the right DDM in the Doppler interval [-5.0,4.5] Hz is null, proving that DDM compression is invariant for Doppler frequency values at the SP that are integer multiples of the Doppler bin size. The x-axis values are Doppler frequencies relative to the Doppler frequency at the SP used for the DDM compression.

The left plots of Figures 5 and 6 represent two DDMs obtained by compressing the raw echo at the first instant of time of the red track depicted in Figure 2 (cyan point) with a different value of the Doppler frequency at the SP. The DDM of Figure 5 (6) is obtained by convolving the raw echo with the on-board (most accurate) estimate of the Doppler frequency at the SP. The right plots of figures 5 and 6 represent the normalized WFs at ± 1 kHz (black and red, respectively) for the two cases, together with their cross-correlation value, as from the QC scheme used in (Grieco, 2018). It is evident, that in Figure 6, the WFs are better aligned than in Figure 5. Indeed, in Figure 5, the WF at 1 kHz arrives before the WF at -1 kHz, while in Figure 6 WFs are more synchronized. Furthermore, by zooming in the WFs plot of Figure 5, one can appreciate that even the LESs are different, while in Figure 6 they are very similar. This aspect is confirmed also by the value of ρ , which is higher in Figure 6. Note that the differences between the trailing edges of the WFs are mainly geophysical, since different magnitudes of the WFs can be related to differences in σ_0 , and therefore in mean square slope (which is mainly related to wind speed). Here, the focus is on the DDM shape and not on its magnitude differences. It has been verified that for the entire tracks analysed in this study, the ρ value is higher when the most accurate estimate of the Doppler frequency at the SP is used instead of the on-board estimate, which leads to conclude that the distortions can be reduced with a more appropriate processing.

One should also consider that any relative WF delay shift in the Doppler interval [-1,1] kHz affects the estimation of the DDMA. It is important to remind here that DDMA and LES are the observables used in the CYGNSS operational wind speed retrieval algorithm. The effects of such distortions on both

observables and on the retrievals will be assessed in the future. Finally, it is recommended that the level 0 data (raw echoes) become operationally available to the scientific community in future satellite GNSS-R missions.

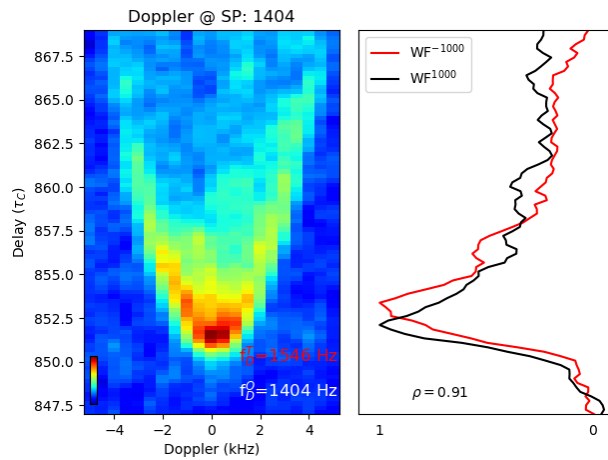


Figure 5: Left: DDM obtained by compressing the raw echo with the on-board estimate of the Doppler frequency at the SP (f_D^0). Right: Normalized WFs at 1 kHz (-1 kHz) in black (red). ρ is the cross correlation coefficient of the two WFs.

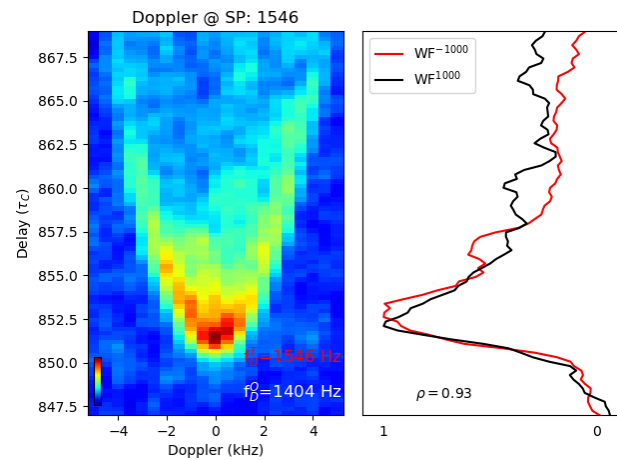


Figure 6: Left: DDM obtained by compressing the raw echo with the most accurate available estimate of the Doppler frequency at the SP (f_D^T). Right: Normalized WFs at 1 kHz (-1 kHz) in black (red). ρ is the cross correlation coefficient of the two WFs.

REFERENCES

- Cardinali, C., (2009) "Monitoring the observation impact on the shortrange forecast". Quarterly Journal of the Royal Meteorological Society, **135**, 638, pp. 239–250, 2009
- Clarizia, M. P., Ruf, C. S., Jales, P., and Gommenginger, C., (2014) "Spaceborne gnss-r minimum variance wind speed estimator". IEEE Transactions on Geoscience and Remote Sensing, **52**, 11, pp. 6829–6843
- Foti, G., Gommenginger, C., Jales, P., Unwin, M., Shaw, A., Robertson, C., and Rosell, J., (2015) "Spaceborne gnss reflectometry for ocean winds: First results from the uk techdemosat1 mission". Geophysical Research Letters, **42**, 13, pp. 5435–5441
- Grieco, G., Stoffelen, A., Portabella, M., Belmonte Rivas, M., Lin, W., Fabra, F., (2018) "Quality control of delay-Doppler maps for stare processing". IEEE Transactions on Geophysical Remote Sensing, "Under review"
- Rodriguez-Alvarez, N. and Garrison, J. L., (2016) "Generalized linear observables for ocean wind retrieval from calibrated gnss-r delay Doppler maps". IEEE Transactions on Geoscience and Remote Sensing, **54**, 2, pp. 1142–1155
- Tye, J., Jales, P., Unwin, M. and Underwood, C., (2016) "The first application of stare processing to retrieve mean square slope using the sgr-resi gnss-r experiment on tds-1". IEEE Journal of Selected Topics in Applied Earth Observations and Remote Sensing, **9**, 10, pp. 4669–4677
- Zavorotny, V. U. and Voronovich, A. G., (2000) "Scattering of gps signals from the ocean with wind remote sensing application". IEEE Transactions on Geoscience and Remote Sensing, **38**, 2, pp. 951–964